

Transient flows in active porous media

Lefteris I. Kosmidis and Kaare H. Jensen*

Department of Physics, Technical University of Denmark, Kgs. Lyngby, DK-2800, Denmark

(Received 3 February 2017; published 26 June 2017)

Stimuli-responsive materials that modify their shape in response to changes in environmental conditions—such as solute concentration, temperature, pH, and stress—are widespread in nature and technology. Applications include micro- and nanoporous materials used in filtration and flow control. The physiochemical mechanisms that induce internal volume modifications have been widely studied. The coupling between induced volume changes and solute transport through porous materials, however, is not well understood. Here, we consider advective and diffusive transport through a small channel linking two large reservoirs. A section of stimulus-responsive material regulates the channel permeability, which is a function of the local solute concentration. We derive an exact solution to the coupled transport problem and demonstrate the existence of a flow regime in which the steady state is reached via a damped oscillation around the equilibrium concentration value. Finally, the feasibility of an experimental observation of the phenomena is discussed.

DOI: [10.1103/PhysRevE.95.062608](https://doi.org/10.1103/PhysRevE.95.062608)**I. INTRODUCTION**

Fluid flow and convective solute transport in porous media and confined channel geometries are ubiquitous in nature and technology. Interesting phenomena arise when channel walls and solid structures are themselves active, for instance when the presence of solutes influences the channel geometry and hence permeability to fluid flow. Man-made examples include sensing and actuation in microfluidic systems using stimuli-responsive hydrogels [1]. Responsive biomaterials are found, for example, in the phloem and xylem vascular systems of plants, where neighboring cells are separated by planar membranes covered with pores that respond to changes in concentration of chemical signals [2,3]. The stimuli that induce changes in these synthetic and natural materials have been widely studied. However, the coupling between induced volume changes and advective solute transport in porous materials is not well understood.

In this paper, we investigate the transient nature of advective transport in active porous media. We study a one-dimensional system in which the advective solute transport speed is coupled to the concentration field. Numerical investigation of the model reveals the existence of a flow regime in which the steady state is reached via a damped oscillation around the equilibrium concentration value. We derive an exact solution using perturbation theory and show that the flow dynamics depends primarily on the ratio of advective to diffusive transport time scales (the Peclet number, Pe). Above a critical Pe value, damped oscillations occur in both the velocity and concentration fields. Finally, we propose an experimental design to test the theoretical predictions.

II. FLOWS IN ACTIVE POROUS MEDIA

Stimulus-responsive hydrogels have been a topic of extensive research in the past few decades [1]. Their ability to modify their internal structure based on external stimuli allows for dynamic control over flows in biological [2,3]

or man-made systems [1,4] (Fig. 1). Responsive hydrogels, i.e., hydrophilic polymers embedded and cross-linked into hydrophilic structures [4], can respond to a broad range of stimuli, e.g., pH [5–13], temperature [14,15], individual molecules (chemically driven) [16–19], shear stress [20–25], etc., that trigger a change of material properties. In pH-induced responses, hydrogel swelling and deswelling occurs when polymers are ionized by the dynamically changing environmental pH [5]. Hence, the charge buildup results in an electrostatic force generation within the hydrogel that ultimately leads to absorbance or expulsion of water [6,7]. Other workers have investigated temperature-dependent hydrogels utilizing the critical solubility temperature with applications in drug delivery [14] and tissue engineering [15]. Hydrogels also exhibit responsive behavior to chemical stimuli such as glucose by entrapping glucose oxidase enzymes in the hydrogel structure [16]. Another group of stimulus-responsive hydrogels are known to respond to mechanical stress. Two subgroups that emerge are materials with shear thinning or shear thickening behavior due to the viscoelastic nature of systems comprised of polymers, an intermediate material state at the interface between liquids and solids [20,21]. Applications of shear stress responsive hydrogels include, among others, drug delivery and wound repair [22–25].

In summary, the physiochemical factors that induce volume changes in stimulus-responsive materials are well understood. By contrast, less is known about the coupling between fluid flow, solute advection, and stimulus response in these systems.

III. MODEL

To elucidate the transient behavior of flow in active porous media, we consider flow in a long and narrow channel of constant cross section aligned with the horizontal X axis linking two large reservoirs (Fig. 2). The channel has length L , width $w \ll L$, and height $h \ll L$, and a short section of active porous media is located at $X = X_0 < L$. The right reservoir ($X = L$) is kept at constant concentration C_0 , while the left reservoir ($X = 0$) contains no solute. This drives a diffusive flux $-D\nabla C$ in the channel, where D is the diffusion coefficient. The right reservoir ($X = L$) is kept at constant

*khjensen@fysik.dtu.dk

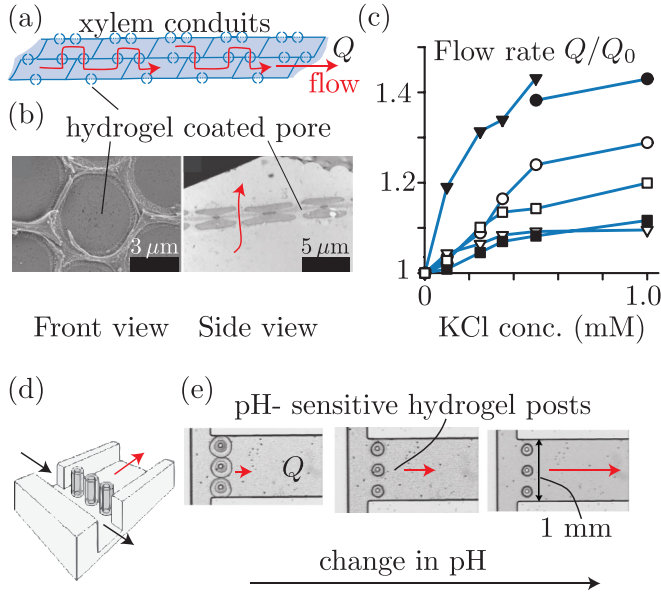


FIG. 1. Examples of active porous media in nature and technology. (a),(b) Sketch and electron micrographs of hydrogel-coated pores that separate xylem conduits in vascular plants. (c) The flow rate Q through the conduits depends on the concentration of KCl, which influences the hydrogel permeability. Lines represent flow through different xylem samples. (d),(e) Sketch and micrographs of a concentration-dependent microfluidic valve. The valve comprises pH-sensitive hydrogel posts that shrink and swell in response to local pH. Panel (b) adapted from [26], (c) from [2], and (d),(e) from [27]. Reproduced with permission from copyright holders.

pressure p_0 , while the left reservoir ($x = 0$) is at a higher pressure $p_0 + \Delta p$. We assume the advective flow speed in the channel v follows Darcy's law, $v \sim \kappa \Delta p / (\eta L)$, where κ is the channel permeability and η is the viscosity. To model the active porous media, we assume that the dependence of the channel permeability κ on solute concentration c can be expressed as $\kappa = \kappa_0 C(X_0) / C_0$. The hydraulic conductivity is proportional to the concentration at the location of the active porous media, X_0 , such that high solute concentration evokes deswelling of the post valves while low concentration leads to an increase of post valve volume (Fig. 2).

The transport of solutes in the channel is governed by the advection-diffusion equation

$$\partial_T C + \mathbf{v} \cdot \nabla C = D \nabla^2 C, \quad (1)$$

where T is time, \mathbf{v} is the velocity field, and D is the diffusion coefficient. We reduce the spatial complexity by considering the limit where the concentration only varies along the X axis, i.e., $C(X, Y, Z, T) = C(X, T)$. This assumes that the time for transverse diffusion is smaller than axial diffusion and advection times. Specifically, we require that h^2/D and w^2/D are smaller than L^2/D and L/v . In terms of geometric and flow constraints, this can be expressed as the channel having a sufficiently small aspect ratio (h^2/L^2 and $w^2/L^2 < 1$) and that the flow speed v is sufficiently slow to allow for transverse diffusive equilibration h^2/L^2 and $w^2/L^2 < D/(vL)$.

With the aforementioned assumptions, Eq. (1) reduces to a one-dimensional equation for the concentration $C(X, T)$ in the

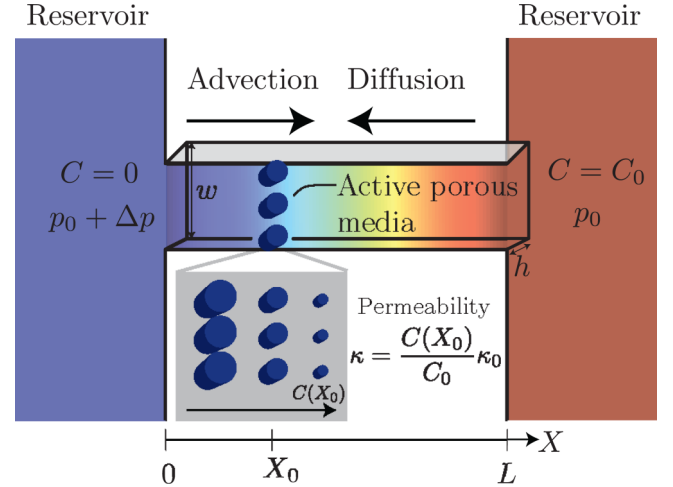


FIG. 2. Schematic illustration of the system. A small channel of length L , width w , and height h link two large reservoirs. Differences in pressure (Δp) and solute concentration ($\Delta C = C_0$) drive advective and diffusive transport of solute in opposite directions through the channel (large arrows). The active porous media pillars located at X_0 swell and shrink in inverse proportion to the local solute concentration (inset). This coupling between flow and concentration is modeled by concentration-dependent Darcy permeability $\kappa = \kappa_0 C(X_0) / C_0$.

channel

$$\partial_T C + \frac{\kappa_0 \Delta p}{\eta L} \frac{C(C_0)}{C_0} \partial_X C = D \partial_X^2 C. \quad (2)$$

The boundary conditions are

$$C(0) = 0, \quad C(L) = C_0. \quad (3)$$

For convenience we introduce the nondimensional variables

$$x = X/L, \quad c = C/C_0, \quad \text{and} \quad t = T(D/L^2). \quad (4)$$

The dimensionless governing equation is

$$\partial_t c + \text{Pe} c(x_0) \partial_x c = \partial_x^2 c, \quad (5)$$

where $x_0 = X_0/L$ and we have introduced the dimensionless Peclet number $\text{Pe} = v_0 L / D$. Here, $v_0 = \kappa_0 \Delta p / (\eta L)$ is the maximum reference velocity. The Peclet number characterizes the relative contribution from advective and diffusive transport. The boundary conditions in Eq. (3) become

$$c(0) = 0, \quad c(1) = 1. \quad (6)$$

In the following, we consider the initial condition corresponding to an empty channel:

$$c(x, 0) = 0, \quad (7)$$

and we study the transient dynamics of the system. Before proceeding, however, we briefly discuss the steady-state solution $c_s(x)$ to Eq. (5) and the system behavior when $\text{Pe} \ll 1$.

A. Steady-state solution

When $\partial_t c = 0$, Eq. (5) reduces to

$$\text{Pe} \gamma \partial_x c_s(x) = \partial_x^2 c_s(x), \quad (8)$$

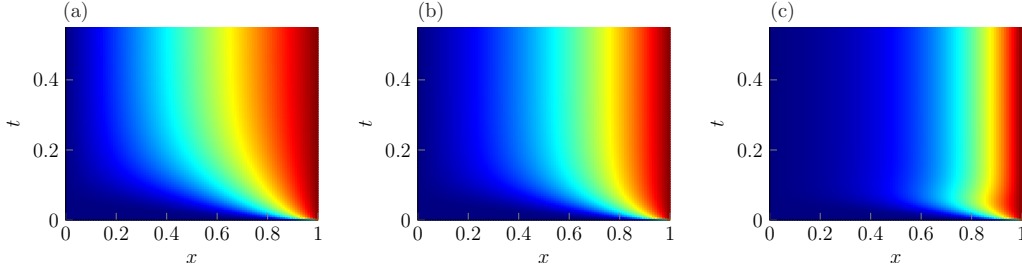


FIG. 3. Oscillations in active porous media at high Pe. Kymographs of the transient evolution of the solute concentration $c(x,t)$ in the pipe for Peclet numbers increasing from left to right: Pe = 1 (a), Pe = 10 (b), and Pe = 100 (c). The active porous media is located at $x_0 = 0.25$. Colors indicate concentration (dark blue: $c = 0$, dark red: $c = 1$).

where we have introduced the parameter $\gamma = c_s(x_0)$, the steady-state concentration at x_0 . The solution to Eq. (8) with boundary conditions (6) is

$$c_s(x) = \frac{e^{\text{Pe}\gamma x} - 1}{e^{\text{Pe}\gamma} - 1}. \quad (9)$$

The parameter $\gamma = c_s(x_0)$ can be determined as a function of the system parameters (Pe and x_0) by solving the transcendental equation

$$\gamma = \frac{e^{\text{Pe}\gamma x_0} - 1}{e^{\text{Pe}\gamma} - 1}. \quad (10)$$

When $\text{Pe} \ll 1$, we find that $c(x) = x$ and $\gamma = x_0$. Taking the limit $\text{Pe} \gg 1$ leads to $\log \gamma / \gamma = \text{Pe}(x_0 - 1)$

B. Solution in a diffusion-dominated system

When diffusion dominates, the Peclet number $\text{Pe} \ll 1$. In that limit, the solution to Eqs. (5) and (6) is

$$c(x,t) = x + \frac{2}{\pi} \sum_n \frac{(-1)^n}{n} \exp^{-n^2\pi^2 t} \sin(n\pi x). \quad (11)$$

Equilibrium is approached exponentially on the time scale set by the slowest mode ($n = 1$). The system is within 5% of the steady-state solution when $t \simeq 3\pi^{-2} \simeq 0.3$.

IV. RESULTS

A. Numerical simulation

To reveal the transient nature of flow in active porous media (Fig. 2), we ran simulations of Eqs. (5)–(7) for a range of values for Pe and x_0 . For relatively low Peclet numbers—corresponding to a diffusion-dominated system—the steady state is reached asymptotically with nondimensional relaxation time $\tau \sim 0.3$ [Figs. 3(a) and 3(b)]. The behavior of the system is thus in accord with a purely diffusive process [Eq. (11)], where equilibrium is approached exponentially on a similar time scale.

By contrast, for large values of the Peclet number Pe above unity, the characteristics of the system change in two respects. First, the steady state is reached on a time scale that decreases with increasing Pe. Second, for large Pe the approach to equilibrium follows a damped oscillation [Fig. 3(c)], indicating a qualitative deviation from the asymptotic approach to equilibrium in Eq. (11) and Fig. 3(a).

To further elucidate the characteristics of the oscillations, we studied the temporal evolution of a small disturbance to the steady state. We thus added a weak Gaussian perturbation to the steady-state solution [Eq. (9)] at an arbitrary position x_p within the domain, and we studied the approach to equilibrium. The amplitude of the perturbation was less than 3% of the steady-state value. After the initial perturbation had decayed, we observed an approximately decaying harmonic time dependence of the disturbance at the position x_{obs} , i.e.,

$$c(x_{\text{obs}}, t) - c_s(x_{\text{obs}}) \propto e^{-(k_r + ik_i)t}, \quad (12)$$

where c_s is the steady-state concentration given in Eq. (9). In Eq. (12), k_r and k_i are the real and imaginary parts of the complex wave number k , corresponding to decay time $\sim k_r^{-1}$ and oscillation period $\sim 2\pi k_i^{-1}$. We thus extracted k_r and k_i from the numerical simulations by curve fitting using the FMINSEARCH package of MATLAB (The Mathworks, Inc., MA). Neither the position of the perturbation x_p nor the observation location x_{obs} appeared to influence the magnitude of the wave number k significantly. However, we chose the parameters to avoid overlap between the position of the active porous material x_0 and x_p and x_{obs} . Finally, we found that while oscillations are present when the position is to the right of the channel centerline ($x_0 > 1/2$), they decay rapidly and a sum of at least two decaying exponentials is necessary to provide a satisfactory curve fit. In the following, we thus restrict ourselves to the case $x_0 < 1/2$.

Having extracted the wave number $k = k_r + ik_i$ from the numerical simulations, we studied k 's dependence on the relative importance of advection and diffusion (Fig. 4). When the Peclet number is relatively small, we found $k_r \simeq 10$ and $k_i = 0$, in accord with Eq. (11), which predicts $k_r = 1^2\pi^2 \simeq 9.87$ and $k_i = 0$. The simulations further revealed that the onset of oscillations occurs at a critical value of the Peclet number Pe_c . For the case $x_0 = 1/4$ shown in Fig. 4, $\text{Pe}_c \simeq 20$. Note that the magnitude of the critical Pe_c varies depending on the location x_0 of the active porous media in the channel (see also Fig. 6).

The physical mechanism that triggers the onset of oscillations can be interpreted as follows: when the system is perturbed away from the steady state $c_s(x)$, the concentration at x_0 , i.e., $c(x_0)$, will shift either up or down as solute is transported by convection through the domain. This directly influences the advective flow speed, which is proportional to the local concentration at that point, $v \propto c(x_0)/c_0$. Diffusion will counteract this process, eventually returning the system

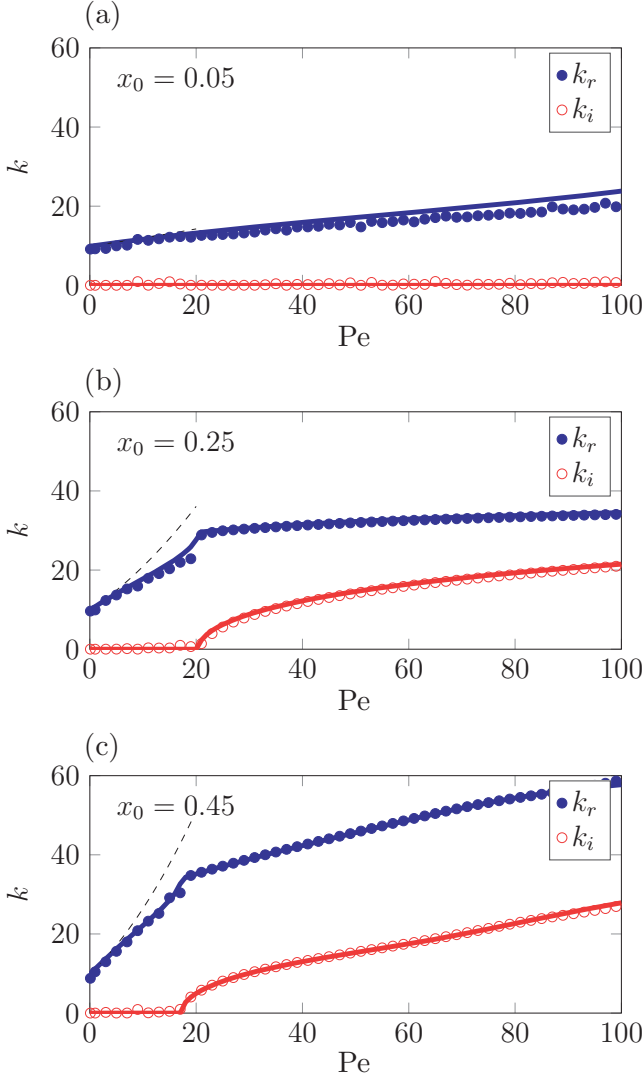


FIG. 4. Onset of oscillations in active porous media with increasing Pe . The real (dots) and imaginary (circle) wave number k plotted as a function of Peclet number Pe for $x_0 = 0.05$ (a), $x_0 = 0.25$ (b), and $x_0 = 0.45$ (c). For $x_0 = 0.25$ [panel (b)], the oscillations appear at $Pe \simeq 20$ where the first nonzero k_i is found. Data points were determined from fits to numerical data (Fig. 3) using Eq. (12). Thick solid lines show results from the analytical solution in Eq. (21). Thin dashed lines indicate the low- Pe limit in Eq. (24).

to the steady state $c_s(x)$. However, if the advective transport is sufficiently strong, advection can push the system into a state in which the concentration gradients become so great that the concentration $c(x_0)$ overshoots its equilibrium value as diffusion counteracts advection. The process repeats itself—with a progressively smaller amplitude—until the steady state is restored.

B. Analytic solution

To rationalize the observed onset of oscillations at high Peclet numbers (Figs. 3 and 4) and their dependence on the system parameters, we proceed to consider the evolution of the perturbed system. Considering a small deviation from the

steady state $c_s(x)$, we write

$$c(x,t) = c_s(x) - c_1(x,t), \quad (13)$$

where we assume the perturbation $c_1 \ll c_s$. We further assume that the perturbation has a harmonic time dependence

$$c_1(x,t) = e^{-kt} g(x), \quad (14)$$

where $k = k_r + ik_i$ is the complex wave number with $k_r > 0$, and $g(x)$ is an unknown function of x . Substitution of Eqs. (14) and (13) into Eq. (5) leads to a spatial equation for $g(x)$,

$$g''(x) - Pe \gamma g'(x) + kg(x) = \frac{Pe^2 \gamma}{e^{Pe \gamma} - 1} e^{Pe \gamma x} g(x_0), \quad (15)$$

where the prime denotes derivative with respect to x . The boundary conditions are

$$g(0) = 0, \quad g(1) = 0, \quad g(x_0) = 1, \quad (16)$$

where we have eliminated quadratic terms in g . Note that $g(x_0)$ is an arbitrary constant that defines the strength of the perturbation, chosen here as unity.

Equation (15) is solved following the method of Pedley and Fischberg [28], who analyzed a similar problem related to transient flows near osmotic membranes. A particular solution to the inhomogeneous equation is $g_i(x) = \lambda \exp(Pe^* x)$, while the homogeneous solution is $g_h = \exp(Pe^* x/2)(A \cos \zeta x + B \sin \zeta x)$. Here, we have introduced the parameters

$$Pe^* = Pe \gamma, \quad (17a)$$

$$\lambda = \frac{1}{k} \frac{Pe^{*2}}{\gamma(e^{Pe^*} - 1)}, \quad (17b)$$

$$\zeta = \frac{1}{2} \sqrt{4k - Pe^{*2}}. \quad (17c)$$

The complete solution to (15) is

$$g(x) = \lambda e^{Pe^* x} + e^{\frac{Pe^* x}{2}} (A \cos \zeta x + B \sin \zeta x). \quad (18)$$

To determine the constants A and B , we apply the boundary conditions

$$g(0) = 0, \quad g(1) = 0, \quad g(x_0) = 1, \quad (19)$$

which after substitution become

$$\lambda + A = 0, \quad (20a)$$

$$\lambda e^{Pe^*} + e^{\frac{Pe^*}{2}} (A \cos \zeta + B \sin \zeta) = 0, \quad (20b)$$

$$\lambda e^{Pe^* x_0} + e^{\frac{Pe^* x_0}{2}} (A \cos \zeta x_0 + B \sin \zeta x_0) = 1. \quad (20c)$$

By eliminating A and B , we find an eigenvalue equation for the wave number k :

$$\lambda e^{\frac{Pe^* x_0}{2}} \left[e^{\frac{Pe^* x_0}{2}} - \cos \zeta x_0 + \frac{\sin \zeta x_0}{\sin \zeta} (\cos \zeta - e^{\frac{Pe^*}{2}}) \right] = 1. \quad (21)$$

To test the validity of our solution, we compared the predictions from Eq. (21) with numerical data. For a given set of parameters (Pe, x_0) we thus determined the solution to Eq. (21) with the smallest real part of k , corresponding to the slowest decaying mode. The solutions to Eq. (21) are in good

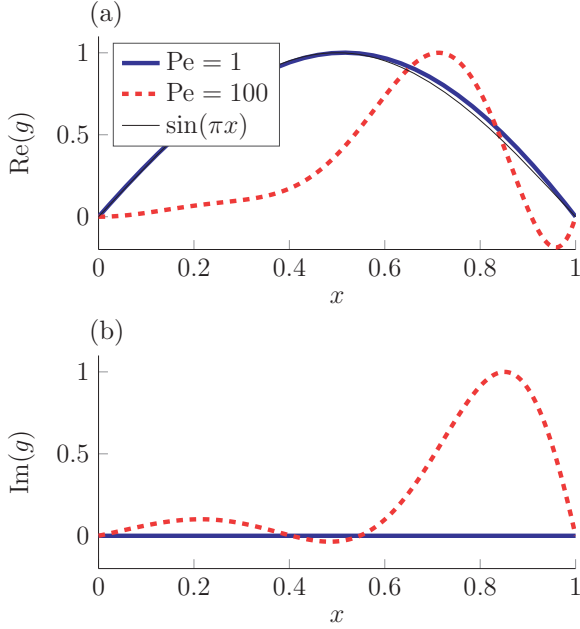


FIG. 5. Eigenfunctions corresponding to Eq. (22) for $x_0 = 0.25$ shown for $Pe = 1$ (thick solid line) and $Pe = 100$ (dashed line). The real part is shown in panel (a), while panel (b) shows the imaginary part. The real eigenfunction [panel (a)] approaches $g \sim \sin \pi x$ in the limit $Pe \rightarrow 0$ (thin solid line), in accord with Eq. (11).

agreement with the numerically extracted eigenvalues (Fig. 4). The eigenfunction is

$$g(x) = \lambda \left\{ e^{Pe^* x} + e^{\frac{Pe^* x}{2}} \left[-\cos \zeta x + \left(\cot \zeta - \frac{e^{\frac{Pe^* x}{2}}}{\sin \zeta} \right) \sin \zeta x \right] \right\}, \quad (22)$$

shown in Fig. 5. We note that the spatial eigenfunctions in Eq. (22) are consistent with Eq. (11) when Pe is relatively small.

C. Critical Pe for the onset of oscillations

To elucidate the conditions under which damped oscillations occur in our system, we extracted a phase diagram (Fig. 6) from the eigenvalue equation (21). Oscillations in the mode associated with the smallest real eigenvalue can occur for values for the Peclet number at or above $Pe \simeq 18$, depending on the position of the active porous media x_0 . This suggests that advection should be nearly 20 times stronger than diffusion to obtain oscillations. However, because of the coupling between the permeability of the porous media, $\kappa = \kappa_0 c(x_0)/c_0 = \kappa \gamma$, and concentration $c(x_0)$, we can write for the flow speed $v = \kappa \Delta p / (\eta L) = \gamma v_0$. This implies that the physically relevant Peclet number is Pe^* , given by

$$Pe^* = \frac{v}{v_0} Pe = \gamma Pe. \quad (23)$$

Replotting the phase diagram using the rescaled Peclet number Pe^* reveals that the onset of oscillations occurs when advection is two to four times stronger than diffusion.

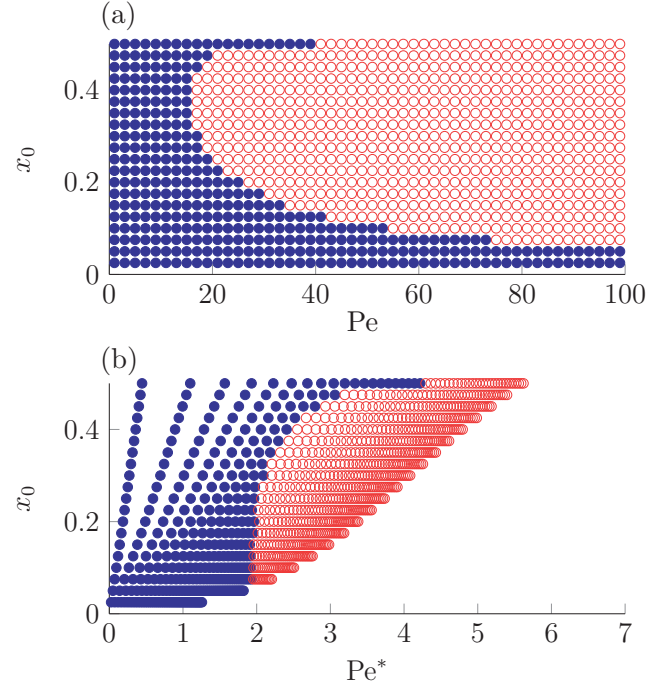


FIG. 6. Phase diagrams showing the system behavior as a function of the Peclet number Pe , panel (a)] and the rescaled Peclet number Pe^* , panel (b)] and the position of the active porous material x_0 . Blue dots indicate the absence of oscillations ($k_i = 0$), while red circles correspond to parameter choices at which oscillations are observed. The onset of oscillations occurs at or above $Pe \simeq 18$ and $Pe^* \simeq 2$, depending on the location of the active porous material x_0 .

Oscillations are found in the numerical simulations for $x_0 > 1/2$. As noted earlier, however, they decay rapidly and a sum of at least two decaying exponentials is necessary to provide a satisfactory curve fit. By extracting the three smallest roots of Eq. (21), we found that for $x_0 > 1/2$ the oscillations are no longer associated with the mode with the smallest real eigenvalue. Oscillations are found, however, in higher-order solutions to Eq. (21), an observation that provides a qualitative rationale for the numerical results.

D. Small- Pe expansion

We end this section by deriving an analytical expression for the solution to Eq. (21) for small Pe . Taking the limit $Pe \ll 1$ in Eq. (20) leads to $\lambda = Pe/k$ and $\zeta = \sqrt{k}$. Inserting this into Eq. (21) and assuming that we can write the eigenvalue as a power series in Pe , $k^{1/2} = a_0 + Pe a_1 + O(Pe^2)$ with $a_0 = \pi$ gives an analytical expression for the eigenvalue k at low Pe ,

$$k(Pe, x_0)^{1/2} = \pi + 2 Pe \frac{\sin(\pi x_0)}{\pi^2} + O(Pe^2). \quad (24)$$

The approximate expression in Eq. (24) is in reasonable accord with the solution to Eq. (21) for $Pe \lesssim 10$ (Fig. 4).

V. DISCUSSION AND CONCLUSION

A relatively complete picture of the factors that influence transient flows in active porous media has emerged. First and foremost, we have demonstrated the existence of damped

oscillations in the flow within a channel linking two reservoirs (Fig. 2). The oscillations in solute concentration and liquid flow speed are the result of a coupling between solute concentration c and the permeability of the channel, controlled by the swelling and shrinking of a stimulus-responsive material located at the position x_0 in the channel. Damped oscillations occur when the advective transport $\sim vc$ is sufficiently great to overcome diffusive transport $\sim Dc/L$, i.e., when the Peclet number $Pe^* = vL/D$ is greater than a critical value, which varies in the range from $Pe^* \simeq 2$ to $Pe^* \simeq 4$, depending on the location of the active porous material x_0 (Fig. 6).

To observe the damped oscillations in a laboratory setting, we propose an experiment based on the system in Fig. 2. In a channel of length $L = 1$ mm, the characteristic diffusive time is $t_d = L^2/D = 2 \times 10^3$ s, where we have used the diffusion coefficient $D = 5 \times 10^{-10}$ m²/s of the dye carboxyfluorescein [29]. With a stimulus-responsive hydrogel valve located at $x_0 = 0.25$ mm operated at a moderate Peclet number of $Pe^* = 4$ ($Pe = 100$), we find $k_r \sim 30$ and $k_i \sim 20$. This corresponds to an oscillation period of $T_{\text{osc}} = 2\pi k_i^{-1} t_d \simeq 630$ s while the decay time is $\tau = 3t_d k_r^{-1} \simeq 200$ s. At least

the first half-period should be observable for this choice of parameters. For a slightly lower forcing $Pe^* = 2$ ($Pe \simeq 30$), we find $k_r \sim 30$ and $k_i \sim 10$ corresponding to oscillation period $T_{\text{osc}} \simeq 1300$ s and decay time $\tau \simeq 200$ s. For water flowing in a channel of width $w = 300$ μm and height $h = 100$ μm , these flows would require pressure differentials of $\Delta p = 0.077$ and 0.023 Pa, respectively [30]. These pressure differentials, in the absence of post valves, would generate flow velocities $v_0 = PeD/L = 50$ $\mu\text{m/s}$ and $v_0 = 15$ $\mu\text{m/s}$ for $Pe = 100$ and 30, respectively. However, due to the reduced conductance imposed by the hydrogel structures, the effective velocity for $Pe^* = 4$ is $v = 2$ $\mu\text{m/s}$ and for $Pe^* = 2$ it is $v = 1$ $\mu\text{m/s}$, in accord with the geometric and flow-speed assumptions leading to the one-dimensional model in Eq. (2). In summary, it does not appear technically unfeasible to experimentally validate the existence of damped oscillations in active porous media.

ACKNOWLEDGMENT

This work was supported by a research grant (13166) from VILLUM FONDEN.

-
- [1] M. C. Koetting, J. T. Peters, S. D. Steichen, and N. A. Peppas, *Mater. Sci. Eng., R* **93**, 1 (2015).
 - [2] M. A. Zwieniecki, P. J. Melcher, and N. M. Holbrook, *Science* **291**, 1059 (2001).
 - [3] D. L. Mullendore, C. W. Windt, H. Van As, and M. Knoblauch, *The Plant Cell* **22**, 579 (2010).
 - [4] M. R. Huglin, *Brit. Polymer J.* **21**, 184 (1989).
 - [5] P. Gupta, K. Vermani, and S. Garg, *Drug Discovery Today* **7**, 569 (2002).
 - [6] L. A. Sharpe, A. M. Daily, S. D. Horava, and N. A. Peppas, *Exp. Opin. Drug Delivery* **11**, 901 (2014).
 - [7] L. A. Sharpe, A. M. Daily, S. D. Horava, and N. A. Peppas, *Eur. J. Pharmaceutics Biopharmaceutics* **50**, 27 (2000).
 - [8] H.-Y. Park, I.-H. Song, J.-H. Kim, and W.-S. Kim, *Int. J. Pharmaceutics* **175**, 231 (1998).
 - [9] A. W. Chan, R. A. Whitney, and R. J. Neufeld, *Biomacromolecules* **9**, 2536 (2008).
 - [10] A. W. Chan and R. J. Neufeld, *Biomaterials* **30**, 6119 (2009).
 - [11] S. Y. Kim, S. M. Cho, Y. M. Lee, and S. J. Kim, *J. Appl. Polym. Sci.* **78**, 1381 (2000).
 - [12] X. Qu, A. Wirsan, and A.-C. Albertsson, *Polymer* **41**, 4589 (2000).
 - [13] D. Schmaljohann, *Adv. Drug Delivery Rev.* **58**, 1655 (2006), Supplementary Non-Thematic Collection.
 - [14] L. Klouda and A. G. Mikos, *Eur. J. Pharmaceutics Biopharmaceutics* **68**, 34 (2008), interactive Polymers for Pharmaceutical and Biomedical Applications.
 - [15] S. Purushotham and R. Ramanujan, *Acta Biomater.* **6**, 502 (2010).
 - [16] Q. Wu, L. Wang, H. Yu, J. Wang, and Z. Chen, *Chem. Rev.* **111**, 7855 (2011).
 - [17] P. Bernfeld and J. Wan, *Science* **142**, 678 (1963).
 - [18] T. A. Horbett, J. Kost, and B. D. Ratner, Swelling Behavior of Glucose Sensitive Membranes, in *Polymers as Biomaterials* (Springer, Boston, 1984), pp. 193–207.
 - [19] L. A. Klumb and T. A. Horbett, *J. Controll. Release* **18**, 59 (1992).
 - [20] A. S. Hoffman, *Adv. Drug Delivery Rev.* **65**, 10 (2013), advanced Drug Delivery: Perspectives and Prospects.
 - [21] Y. Qiu and K. Park, *Adv. Drug Delivery Rev.* **53**, 321 (2001), triggering in Drug Delivery Systems.
 - [22] Q. Wang, L. Wang, M. Detamore, and C. Berkland, *Adv. Mater.* **20**, 236 (2008).
 - [23] C. J. Bell, L. M. Carrick, J. Katta, Z. Jin, E. Ingham, A. Aggeli, N. Boden, T. A. Waigh, and J. Fisher, *J. Biomed. Mater. Res. A* **78A**, 236 (2006).
 - [24] M. Guvendiren, H. D. Lu, and J. A. Burdick, *Soft Matter* **8**, 260 (2012).
 - [25] A. Gutowska, B. Jeong, and M. Jasionowski, *Anatom. Rec.* **263**, 342 (2001).
 - [26] B. Choat, A. R. Cobb, and S. Jansen, *New Phytologist* **177**, 608 (2008).
 - [27] D. J. Beebe, J. S. Moore, J. M. Bauer, Q. Yu, R. H. Liu, C. Devadoss, and B.-H. Jo, *Nature (London)* **404**, 588 (2000).
 - [28] T. Pedley and J. Fischbarg, *J. Theor. Biol.* **70**, 427 (1978).
 - [29] N. J. Carroll, K. H. Jensen, S. Parsa, N. M. Holbrook, and D. A. Weitz, *Langmuir* **30**, 4868 (2014).
 - [30] H. Bruus, *Theoretical Microfluidics* (Oxford University Press, Oxford, 2007).